Slip flow in elliptic microducts with constant heat flux

Hindawi Publishing Corporation
Advances in Mechanical Engineering
Volume 2012, Article ID 481280, 8 pages
doi:10.1155/2012/481280

*Research Article*

# Slip Flow in Elliptic Microducts with Constant Heat Flux

**Marco Spiga and Pamela Vocale**

*Department of Industrial Engineering, University of Parma, Parco Area delle Scienze 181/A, 43124 Parma, Italy*

Correspondence should be addressed to Marco Spiga, marco.spiga@unipr.it

Received 28 April 2012; Revised 6 September 2012; Accepted 10 September 2012

Academic Editor: C. T. Nguyen



This paper outlines a numerical model for determining the dynamic and thermal performances of a rarefied fluid flowing in a microduct with elliptical cross-section. A slip flow is considered, in laminar steady state condition, in fully developed forced convection, with Knudsen number in the range $0.001-0.1$, in H1 boundary conditions. The velocity and temperature distributions are determined in the elliptic cross-section, for different values of both aspect ratio $\gamma$ and Knudsen number, resorting to the Comsol Multiphysics software, to solve the momentum and energy equations. The friction factors (or Poiseuille numbers) and the convective heat transfer coefficients (or Nusselt numbers) are calculated and presented in graphs and tables. The numerical solution is validated resorting to data available in literature for continuum flow in elliptic cross-sections (Kn = 0) and for slip flow in circular ducts ($\gamma = 1$). A further benchmark is carried out for the velocity profile for slip flow in elliptical cross-sections, thanks to a recent analytical solution obtained using elliptic cylinder coordinates and the separation of variables method. The Poiseuille and Nusselt numbers for elliptic cross-sections are discussed. The results may be used to predict pressure drop and heat transfer performance in metallic microducts with elliptic cross-section, produced by microfabrication for microelectromechanical systems (MEMS).

## 1. Introduction

Fluid flow in microchannels has emerged as an important research area. This has been motivated by their various applications such as medical and biomedical use, computer chips, and chemical separations. The advent of microelectromechanical systems (MEMS) has opened up a new research area where noncontinuum behavior is significant.

An important effect associated with gas flows in microchannels, where the typical length scales are measured in microns, is the rarefaction effect. The Knudsen number is a measure of the degree of rarefaction, which is defined as the ratio of the mean free path to the appropriate length scale of the flow. For Knudsen numbers in the range $10^{-3} \leq \mathrm{Kn} \leq 10^{-1}$, deviations from continuum behavior arise near the walls where, in a thin layer, molecular collisions with the walls dominate over intermolecular collisions. This is proved by many experimental works published in the last decades [1–4]. Liu et al. [5] proved that the solution to the Navier Stokes equation, linked to slip flow boundary conditions, shows good agreement with the experimental data.

In the literature, there are several analytical, numerical, and experimental works that deal with the slip flow through microchannels characterized by different geometrical cross-sections as reported in the recent edition of Handbook of Microfluidic and Nanofluidics [6].

Kennard [7] studied internal flows with slip in the circular tube and parallel-plate channel. Sreekanth [8] experimentally investigated slip flow through long circular microtubes and proposed a second-order slip boundary condition according to the pressure distribution along the microtube. The effects of the Reynolds number and the Knudsen number on the hydrodynamic development lengths in circular and parallel plate ducts was investigated by Barber and Emerson [9].

Ebert and Sparrow [10] performed an analysis to determine the velocity and pressure drop characteristics of slip flow in rectangular and annular ducts. They found that the effect of slip is to flatten the velocity distribution relative to that of a continuum flow and that the compressibility increases the pressure drop through an increase in the viscous shear rather than through an increase in the momentum

flux. Recently, their solution has been re-examined by Duan and Muzychka [11] in order to investigate slip flow in noncircular microchannels. They developed a simple model for predicting the friction factor-Reynolds product in noncircular microchannels for slip flow. The proposed model took advantage of the selection of a more appropriate characteristic length scale (square root of flow area) to develop a simple model. The accuracy of the developed model was found to be within 10%, with most data for practical configurations within 5%.

Slip flow in rectangular microchannel was also investigated by Morini et al. [12–14]. They presented the 2D velocity distribution of steady-state, hydrodynamically developed, laminar slip flow, for Newtonian fluids in rectangular ducts [12]. They also pointed out the roles of the Knudsen number and the cross-section aspect ratio in the friction factor reduction due to the rarefaction [13]. They found that for rectangular microchannels with a small aspect ratio the decrease of the friction factor with the Knudsen number is larger. In other words, the rarefaction effects appear to be higher in microchannels with smaller aspect ratios.

Yu and Ameel [15] studied slip flow heat transfer in microchannels and found that heat transfer increases, decreases, or remains unchanged, compared to nonslip flow conditions, depending on two dimensionless variables that include effects of rarefaction and fluid/wall interaction.

Aubert and Colin [16] studied slip flow in rectangular microchannels using the second-order boundary conditions proposed by Deissler. In a later study, Colin et al. [17] presented experimental results for nitrogen and helium flows in a series of silicon rectangular microchannels. The authors proposed that the second-order slip flow model is valid for Knudsen numbers up to about 0.25.

Applying the integral transform method, Ghodoossi and Eğrican [18] studied convective heat transfer in a rectangular microchannel under slip flow and H1 boundary condition. They found that rarefaction has a decreasing effect on heat transfer for most engineering microchannel applications, with any aspect ratios.

Renksizbulut et al. [19] examined the effects of rarefaction for simultaneously developing 3D laminar, constant-property flows in rectangular microchannels and for $\mathrm{Kn} \leq 0.1$. They found that slip velocities are significantly reduced in the corner regions as the flow develops along the channel due to weaker velocity gradients. For the range of Reynolds numbers considered in their study, entrance lengths are only marginally influenced by rarefaction effects, but they display a highly nonlinear dependence on the channel aspect ratios.

The effects of rarefaction and aspect ratio on thermal character of flow in rectangular microchannels were also investigated by Kuddusi et al. [20, 21]. They analyzed eight different thermal boundary conditions. Their results show that the highest heat transfer is achieved in the microchannel with two heated long walls and two adiabatic short walls (2L version). The decreasing effect of rarefaction on heat transfer in microchannels, for all the thermal versions, is established. The higher the rarefaction, the lower the heat transfer. Their numerical results also show that heat transfer for the eight thermal versions may increase, decrease, or remain unchanged with aspect ratio. In particular, heat transfer decreases for 1L, 2L, and 3L versions, increases for 1S, 2S, and 3S versions, and it remains approximately unchanged for 4 and 2C versions with increasing aspect ratio.

Slip flow in trapezoidal duct was deeply investigated by Morini et al. [13] and by Kuddusi et al. [22, 23]. Morini carried out a work that deals with the analysis of fully developed laminar liquid flow through silicon microchannels with trapezoidal and double-trapezoidal cross-sections. He found that for the trapezoidal and double-trapezoidal microchannels, the influence of the aspect ratio on the friction factor is strong only if the aspect ratio is less than 0.5.

Kuddusi and Çetegen [22] found that the friction factor decreases if rarefaction and/or aspect ratio increase. He also found that at low rarefactions the very high heat transfer rate at the entrance diminishes rapidly as the thermally developing flow approaches fully developed flow. At high rarefactions, heat transfer rate does not exhibit considerable changes along the microchannel, no matter the flow is thermally developing or not. They also explored the effects of viscous dissipation. They found that heat transfer decreases with rarefaction for common applications ($\mathrm{Br} < 0.005$), while increases with rarefaction at high Brinkman numbers ($\mathrm{Br} > 0.005$). They also observed a decreasing effect of viscous dissipation on heat transfer (up to 60% at high Brinkman numbers).

Only recently a new interest has been devoted to the elliptical cross-section, produced by mechanical fabrication in metallic microducts for practical applications in MEMS (Mechanical Electro Mechanical Systems). An analytical approach, concerning only the dynamic problem and the friction factor for slip flow in elliptical cross-sections, has been presented by Duan and Muzychka [24], using elliptic cylinder coordinates and the separation of variable method. The velocity distribution is given as a series of trigonometric and hyperbolic functions of the spatial coordinates, with coefficients obtained by means of a Fourier expansion. The accuracy of the proposed simple model was found to be within 3 percent of exact values.

In order to analyze flow behavior through microchannel characterized by different cross-section, compact models have been proposed more recently [25–28]. These models use principles of scaling analysis, appropriate selection of characteristic length scales, asymptotic analysis, and nonlinear superposition of asymptotes. A benefit of this new approach is that a significant reduction in the use of graphical and tabulated data arises. Further, because many complex shapes have no analytical solution or numerical data, the models presented in the Handbook of Microfluidic and Nanofluidics [6] act to fill this void and will yield good results in these cases.

To the best of the authors' knowledge, the thermal analysis of slip flow in microchannels of elliptic cross-section is not yet tackled in literature.

The present work is aimed at giving a contribution to the analysis of slip flow through elliptic microchannel, presenting a comprehensive numerical analysis of fully developed flow, in steady state laminar condition under H1

boundary condition. The influence of the aspect ratio and the rarefaction effects on the friction factors (or Poiseuille numbers) and heat transfer coefficients (or Nusselt numbers) is investigated.

## 2. Mathematical Model

Let us consider a gas flowing in a duct with elliptical cross-section, with aspect ratio $\gamma \le 1$ defined as the ratio between minor and major semiaxis.

A Cartesian coordinate system $x$, $y$, $z$ is introduced; the origin is at the centre of the ellipse, and $z$ is horizontal and perpendicular to the channel cross section. The following hypotheses are assumed:

(i) the gas is Newtonian with constant physical properties,

(ii) the walls are rigid and nonporous,

(iii) the flow is forced, in slip flow condition, laminar, hydrodynamically and thermally fully developed,

(iv) the Mach number is low and compressibility effects are negligible,

(v) viscous dissipation, radiative heat transfer, electrostatic interactions, internal heat generation are absent,

(vi) an axial uniform linear heat flux is transferred by the wall at the gas, with isothermal perimeter of the cross-section (H1 boundary condition).

This last hypothesis implies the following balance energy equation between two sections at $z$ and $z + dz$ of the microduct:

$$\frac{\partial T_b}{\partial z} = \frac{q}{\rho c W A}. \tag{1}$$

The hypothesis of fully developed flow implies

$$\frac{\partial T_b}{\partial z} = \frac{\partial T_w}{\partial z} = \frac{\partial T}{\partial z}. \tag{2}$$

Hence, the fluid and wall temperatures present a linear variation along the axis $z$. According to the proposed hypotheses, the classical Navier Stoke and energy equations are

$$\begin{aligned} -\frac{\partial p}{\partial z} + \mu\left(\frac{\partial^2 u}{\partial x^2} + \frac{\partial^2 u}{\partial y^2}\right) &= 0, \\ \frac{q}{A}\frac{u}{W} &= \lambda\left(\frac{\partial^2 T}{\partial x^2} + \frac{\partial^2 T}{\partial y^2}\right). \end{aligned} \tag{3}$$

The following dimensionless independent variables are introduced

$$\xi = \frac{x}{a}, \qquad \psi = \frac{y}{a}, \qquad \zeta = \frac{z}{a} \tag{4}$$

together with the dimensionless dependent functions:

$$p^* = -\frac{a^2}{\mu W}\frac{\partial p}{\partial z}, \qquad U = \frac{u}{W}, \qquad \theta = \frac{\lambda(T - T_w)}{q}. \tag{5}$$

Introducing the dimensionless variables and functions in (3), the dimensionless Navier Stokes and energy equations are

$$\begin{aligned} p^* + \frac{\partial^2 U}{\partial \xi^2} + \frac{\partial^2 U}{\partial \psi^2} &= 0, \\ \frac{\partial^2 \theta}{\partial \xi^2} + \frac{\partial^2 \theta}{\partial \psi^2} &= \frac{1}{\pi\gamma} U. \end{aligned} \tag{6}$$

The first-order slip flow boundary conditions for the dimensionless velocity and temperature at the wall (perimeter of the ellipse) are

$$U_s = \frac{2 - \sigma_v}{\sigma_v}\mathrm{Kn}\frac{D_h}{a}\left(\frac{\partial U}{\partial n}\right)_w = \beta_v \mathrm{Kn}\frac{D_h}{a}\left(\frac{\partial U}{\partial n}\right), \tag{7}$$

$$\theta_j = \frac{2 - \sigma_T}{\sigma_T}\frac{2}{k+1}\frac{k}{\mathrm{Pr}}\frac{\mathrm{Kn}}{\mathrm{Pr}}\frac{D_h}{a}\left(\frac{\partial \theta}{\partial n}\right) = \beta_t \mathrm{Kn}\frac{D_h}{a}\left(\frac{\partial \theta}{\partial n}\right). \tag{8}$$

The Equations (6), linked to the boundary condition (7) and (8), can be solved resorting to the software Comsol Multiphysics 4.2a, a package for engineering applications solving coupled systems of partial differential equations with a finite element analysis. The software package solves the problem in the elliptic domain, with $-1 < \xi < 1$ and $-\gamma < \psi < \gamma$.

If the velocity distribution and temperature are known, the main physical parameters can be deduced. As usual [29], the Poiseuille number is defined as

$$\mathrm{Po} = \frac{\tau D_h}{\mu W} = \frac{\left(-((P)/A)(\partial p/\partial z)\right)D_h}{\mu W} = \frac{D_h^2}{4a^2}p^*. \tag{9}$$

The bulk temperature and the Nusselt number are

$$T_b = \iint \frac{UT}{\pi\gamma} d\xi d\psi, \qquad \mathrm{Nu} = \frac{hD_h}{\lambda} = \frac{D_h}{P|T_b|}. \tag{10}$$

A benchmark can be offered by the analytical solution of the same problem in circular geometry. The well-known solution for slip flow in circular channel under H1 boundary condition, for the velocity distribution, the radial component of temperature and Nusselt number are, respectively:

$$\begin{aligned} U &= \frac{2}{1 + 8\beta_v \mathrm{Kn}}\left(1 + 4\beta_v \mathrm{Kn} - r^{*^2}\right), \\ \theta_r &= \frac{1}{2\pi(1 + 8\beta_v \mathrm{Kn})} \\ &\quad \times \left(\frac{r^{*^4}}{4} - (1 + 4\beta_v \mathrm{Kn})r^{*^2} + 2\beta_t \mathrm{Kn}(1 + 8\beta_v \mathrm{Kn})\right. \\ &\quad \left. + 4\beta_v \mathrm{Kn} + \frac{3}{4}\right) \\ \mathrm{Nu} &= \frac{hD}{\lambda} \\ &= \frac{qD}{\lambda(T_b - T_w)} = \frac{48}{11}\frac{(1 + 8\beta_v \mathrm{Kn})^2}{\mathcal{A}}, \end{aligned} \tag{11}$$

where $\mathcal{A}$ denotes $1 + (128/11)\beta_v \mathrm{Kn}(1 + 3\beta_v \mathrm{Kn}) + (48/11)\beta_t \mathrm{Kn}(1 + 8\beta_v \mathrm{Kn})^2$.

Table 1: Poiseuille numbers for elliptical ducts.

| $\gamma$ | Analytical solution [24] | Present paper | Discrepancy |
|---|---|---|---|
| | Kn = 0.001 | | |
| 0.25 | 9.025 | 9.033 | 0.10% |
| 0.50 | 8.337 | 8.340 | 0.04% |
| 0.75 | 8.015 | 8.020 | 0.07% |
| 1.00 | 7.937 | 7.934 | −0.03% |
| | Kn = 0.01 | | |
| 0.25 | 8.249 | 8.306 | 0.69% |
| 0.50 | 7.718 | 7.739 | 0.27% |
| 0.75 | 7.467 | 7.478 | 0.15% |
| 1.00 | 7.407 | 7.408 | 0.01% |
| | Kn = 0.05 | | |
| 0.25 | 5.969 | 6.125 | 2.61% |
| 0.50 | 5.803 | 5.861 | 0.99% |
| 0.75 | 5.729 | 5.744 | 0.26% |
| 1.00 | 5.714 | 5.713 | −0.02% |
| | Kn = 0.1 | | |
| 0.25 | 4.437 | 4.611 | 3.94% |
| 0.50 | 4.430 | 4.503 | 1.66% |
| 0.75 | 4.437 | 4.459 | 0.49% |
| 1.00 | 4.444 | 4.445 | 0.00% |

## 3. Results and Discussion

The governing equations, together with their boundary conditions, were implemented in Comsol MultiphysicsTM, and they were solved resorting to the parallel sparse direct linear solver MUMPS (multifrontal massively parallel sparse direct Solver), with a relative tolerance set to $1e-06$.

In order to validate the numerical model, the analytical solution proposed by Duan and Muzychka [24] is used as a benchmark. Figure 1 shows the excellent agreement between the numerical results and the analytical ones for aspect ratio set to 0.5; the RMS difference is about 2%. Table 1 shows the comparison between the numerical values of the Poiseuille number and the analytical ones. The numerical results are obtained assuming, for sake of simplicity, $\sigma_v = \sigma_T = 1$, so that there is no difference between the Knudsen number and the modified Knudsen number $\mathrm{Kn}^* = (2-\sigma_v)/\sigma_v$, used in literature by many authors. Moreover the following physical parameters for the gas are chosen, as usual, $\mathrm{Pr} = 0.71$ and $k = 1.4$.

To analyze the sensitivity of the numerical results to the mesh size, five different types of grid configurations are tested. The first four featured a uniform mesh, while the last one was nonuniform, with an enhanced refinement near the wall. The maximum discrepancy, observed in the maximum velocity (calculated in the five different configurations), is less than 2%.

As expected, the nonuniform mesh has the best performance in terms of accuracy. Taking this into account, and considering the small computational effort to run each simulation regardless of the mesh type, the nonuniform configuration is chosen. The adopted mesh is characterized by 13552 triangular elements.

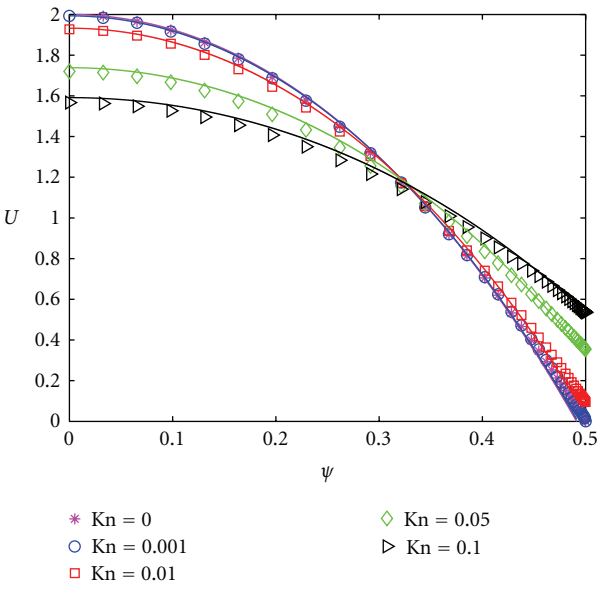


Figure 1: Velocity profiles in elliptic channel for $\gamma = 0.5$.

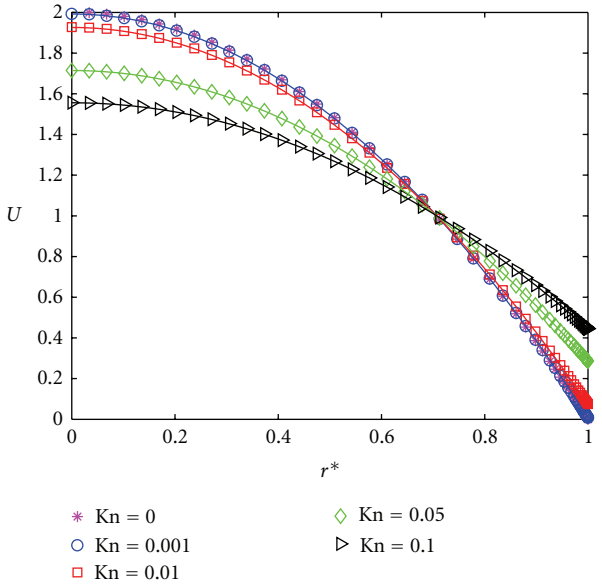


Figure 2: Velocity profiles in circular channel ($\gamma = 1$).

For aspect ratio value set to 1, the numerical results are also compared with analytical values for circular microchannels obtained by (11). Both for velocity field and temperature field, numerical values are in perfect agreement with the analytical ones, as shown in Figures 2 and 3. The RMS differences are less than 0.001% for the velocity profiles and about 0.001% for the temperature distributions.

Table 2 shows the comparison between the numerical values of the Nusselt number and the analytical ones,

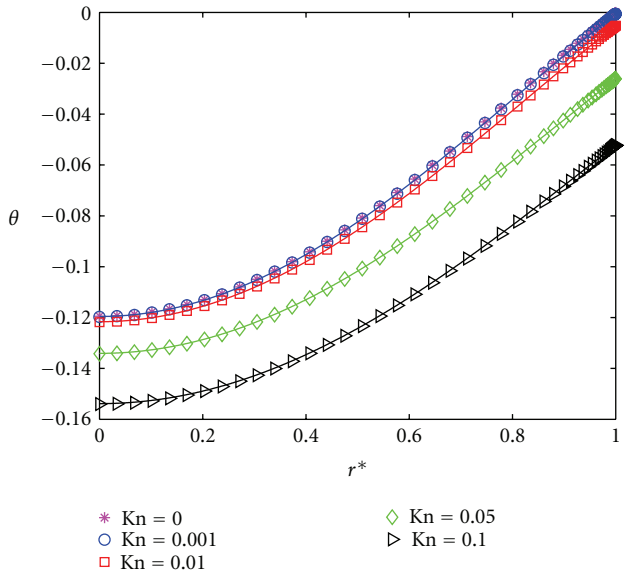


Figure 3: Temperature profiles in circular channel ($\gamma = 1$).

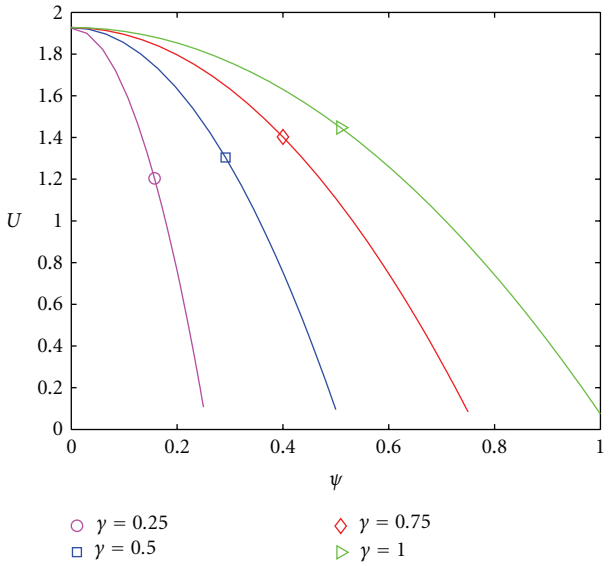


Figure 5: Velocity profiles for Kn = 0.01.

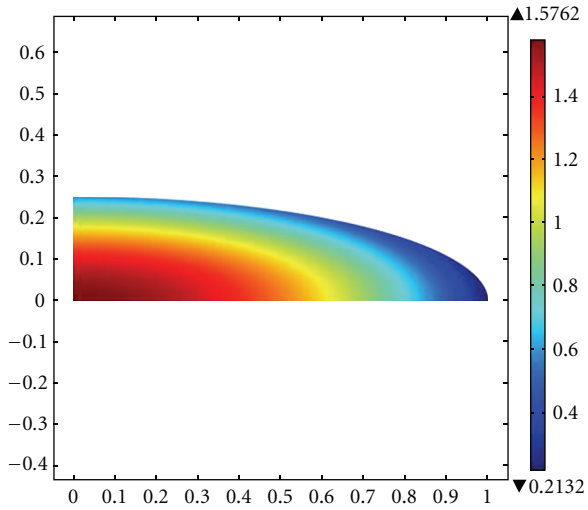


Figure 4: Dimensionless velocity in the cross-section.

Table 2: Nusselt numbers for circular ducts ($\gamma = 1$).

| | Nu (H1) | | |
|---|---|---|---|
| Kn | Analytical solution | Present paper | Discrepancy |
| 0.001 | 4.351 | 4.345 | 0.14% |
| 0.010 | 4.230 | 4.221 | 0.21% |
| 0.050 | 3.609 | 3.604 | 0.14% |
| 0.100 | 2.928 | 2.922 | 0.20% |

emphasizing a high accuracy of the numerical solution, with a discrepancy never greater than 0.21%.

After having tested the reliability and accuracy of the results obtained by the numerical procedure, a general analysis can be proposed and discussed. To cover the most common situations in which elliptical microducts are used, the investigation is carried out assuming the aspect ratio $\gamma$ = 0.25, 0.50, 0.75, and 1.00, and Knudsen number Kn = 0.001, 0.01, 0.05, and 0.1.

Figure 4 presents the spatial distribution of the dimensionless velocity, for $\gamma = 0.25$ and Kn = 0.1, in a quarter of the ellipse (for symmetry reasons); it can be seen that $U$ never goes to 0 because of the slip at the boundary.

The dimensionless velocity profiles are shown in Figure 5, versus the shorter axis of the ellipse, for different values of the aspect ratio.

The numerical results let to state that the continuum flow results (Kn = 0) are extremely close to the results referred to Kn = 0.001. The dimensionless maximum velocity at the centre of the ellipse is determined by the correlation $U_{max} = 26.473\text{Kn}^{*2} - 6.954\text{Kn}^{*} + 2.000$, it does not depend on the aspect ratio of the elliptical cross-section, and for continuum flow it assumes the well-known value of 2. The slip velocity at the wall increases with the Knudsen number; it is higher in $\psi = \pm\gamma$, due to the higher velocity gradient, as stated in (7).

The Poiseuille number is depicted in Figure 6; it is a monotonically slightly decreasing function of $\gamma$, and decreases when the Knudsen number increases. These considerations confirm that the gas rarefaction reduces the friction between the gas and the walls, and microchannels with a small aspect ratio have higher friction factors. The reliability of the numerical solution is again proved by the fact that the Poiseuille numbers are almost identical to the analytical results obtained by the analytical solution available in [24].

The spatial distribution of the dimensionless fluid temperature is shown in Figure 7; the wall has the maximum temperature (being $q < 0$), the minimum temperature is at the centre. Of course, in the more flattened region of the ellipse the temperature is higher.

The dimensionless fluid temperature as a function of the shorter axis $\psi$ is depicted in Figure 8, for Kn = 0.01 and for

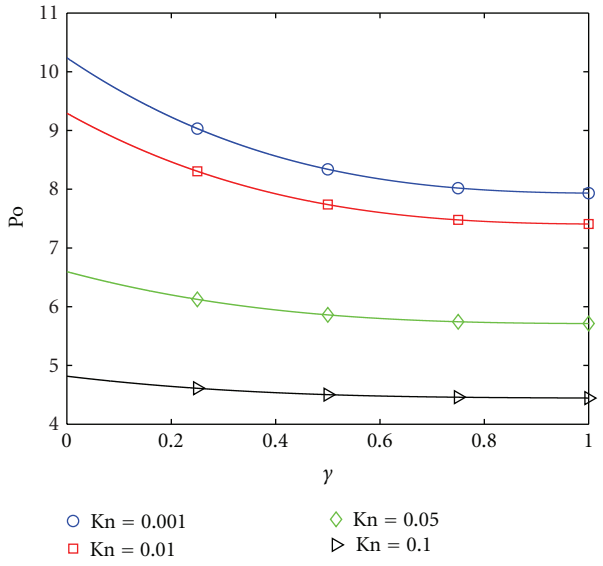


Figure 6: Poiseuille number as a function of aspect ratio, for different Knudsen numbers.

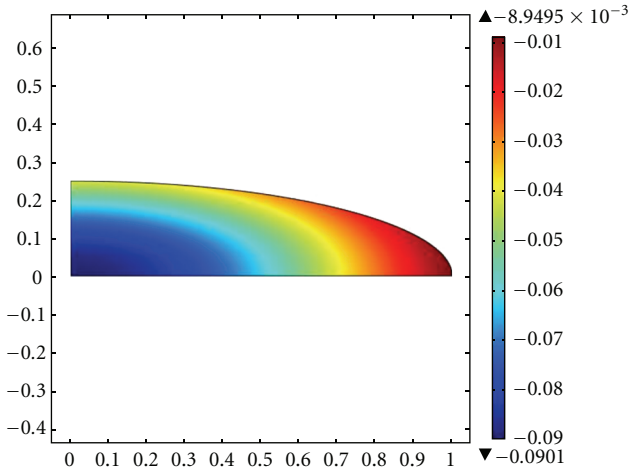


Figure 7: Dimensionless temperature in the cross-section for $\gamma = 0.25$.

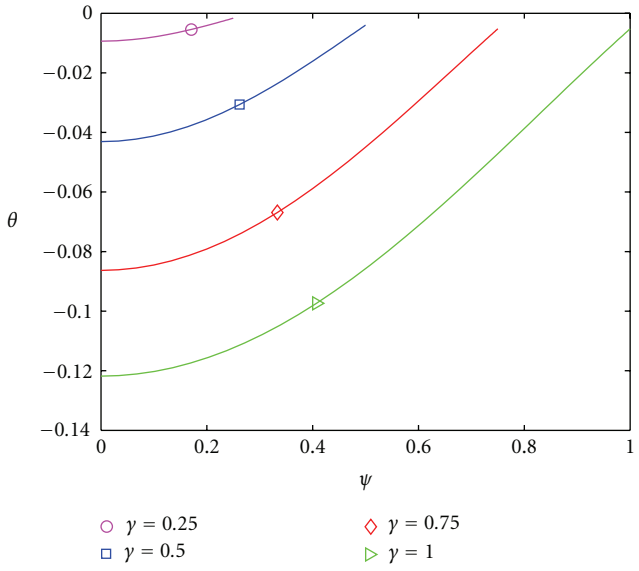


Figure 8: Temperature profiles for Kn = 0.01.

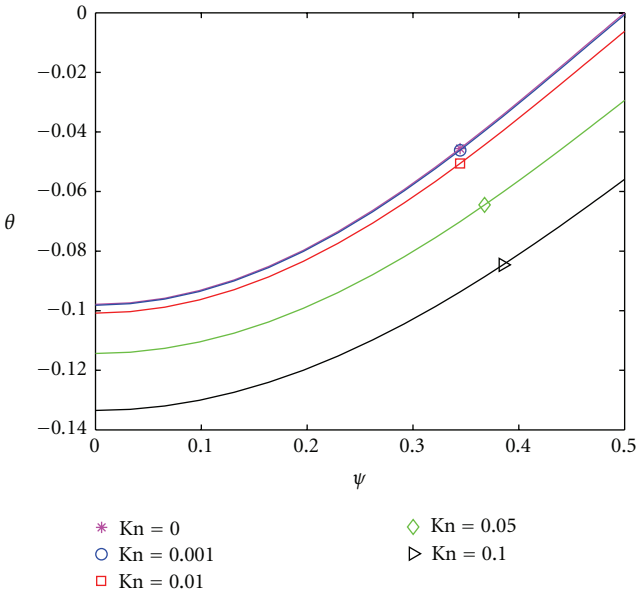


Figure 9: Temperature profiles for $\gamma = 0.5$.

different values of aspect ratio. As the eccentricity increases (i.e., $\gamma$ decreases), the minimum temperature strongly increases, while the temperature jump slightly decrease.

Figure 9 shows the dimensionless temperature profile with $\gamma = 0.5$ along the shorter axis $\psi$, the temperature jump significantly increases with the Knudsen number.

Figure 10 represents the dimensionless bulk temperature profile, it decreases with both aspect ratio and Knudsen number; the circular cross-section is characterized by the lower bulk temperature.

In Figure 11 the effect of both aspect ratio and Knudsen number on the Nusselt number is shown.

The Nusselt number has a curious and unexpected trend. While it strongly decreases monotonically with increasing Knudsen numbers, it shows a contradictory behaviour against the aspect ratio. For low Knudsen numbers, the Nusselt number slightly decreases with increasing of the aspect ratio, for Kn around 0.05 it remains almost unchanged, for Kn $> 0.05$ it increases very slightly with the aspect ratio. Thus the thermal performances are very sensitive to the Knudsen number in slip flow regime, while the aspect ratio plays a minor role in elliptical geometry. For high Knudsen numbers, the effect of the aspect ratio is almost negligible, while for small Knudsen number the eccentricity of the cross-section increases the thermal exchange.

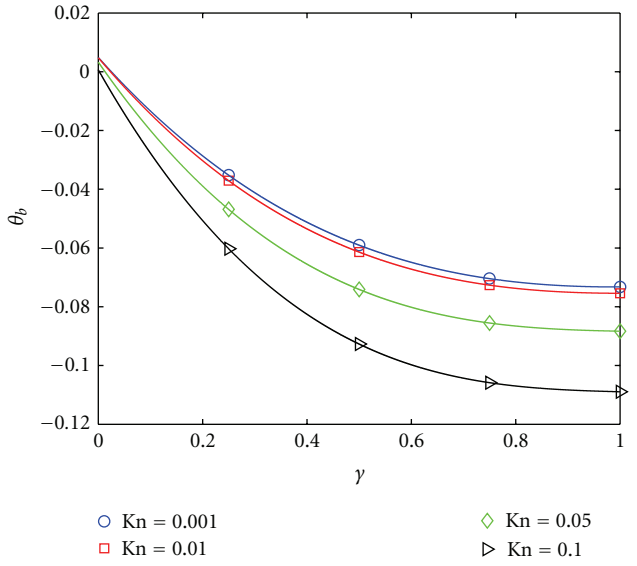


Figure 10: Dimensionless bulk temperature versus $\gamma$ for different Knudsen number.

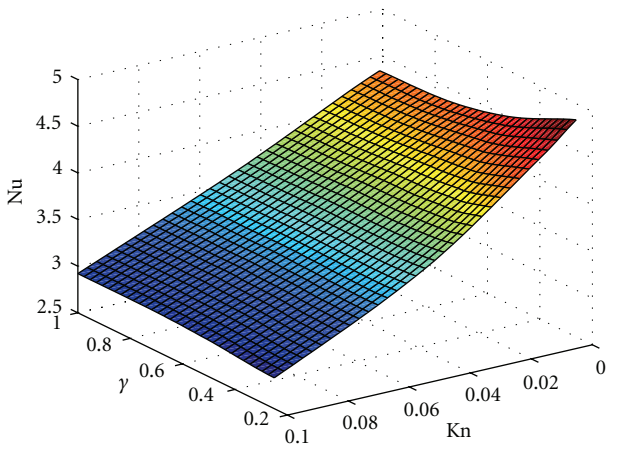


Figure 11: Nusselt numbers versus $\gamma$ for different Knudsen numbers.

Table 3: Polynomial coefficients in (12).

| Kn | $c_0$ | $c_1$ | $c_2$ | $c_3$ |
|---|---|---|---|---|
| 0.001 | 5.4009 | −2.5820 | 2.0133 | −0.4737 |
| 0.010 | 5.0227 | −2.0795 | 1.7532 | −0.4754 |
| 0.050 | 3.7255 | −0.4552 | 0.5932 | −0.2594 |
| 0.100 | 2.7468 | 0.4250 | −0.3128 | 0.0630 |

A simple parabolic form can be proposed to represent Nusselt number as a function of Knudsen number and aspect ratio:

$$\mathrm{Nu} = \sum_{i=0}^{3} c_i \gamma^i, \tag{12}$$

where the values of the constants $c_i$ are listed in Table 3.

In conclusion, the numerical solution presented in this paper allows obtaining fluid velocity and temperature distributions (consequently friction factors and heat transfer coefficients), for slip flow in elliptical microducts with Knudsen numbers in the range 0-0.1 and aspect ratios in the range 0.25–1, in H1 boundary conditions (constant axial flux and isothermal wetted perimeter in each cross-section). To reduce friction losses in microducts, it is convenient to have slip flow with high Knudsen numbers and cross-sections with high aspect ratios (tending to the circular cross-section); on the contrary, the thermal exchange is enhanced for small Knudsen numbers (with minor relevance of the aspect ratio).

## Nomenclature

$A$: Cross-section area, m$^2$
$a$: Semimajor axis of the ellipse, m
$b$: Semiminor axis of the ellipse, m
$c$: Specific heat at constant pressure, J/kg K
$c_v$: Specific heat at constant volume, J/kg K
$D_h$: Hydraulic diameter of the channel, m
$h$: Convective heat transfer coefficient W/m$^2$ K
$k$: Ratio of specific heats, $c/c_v$
Kn: Knudsen number, $\lambda/D$
Kn$^*$: Modified Knudsen number, $\beta_v$ Kn
$n$: Dimensionless normal coordinate at the internal walls of the ellipse
Nu: Nusselt number, $hD_h/\lambda$
$p$: Fluid pressure, Pa
$p^*$: Dimensionless fluid pressure
$P$: Perimeter of the elliptical cross-section, m
Po: Poiseuille number
Pr: Prandtl number
$r^*$: Dimensionless radius
$q$: Constant linear heat flux, W/m
$T$: Fluid temperature, K
$u$: Fluid velocity, m/s
$U$: Dimensionless fluid velocity
$W$: Average velocity, m/s
$x$, $y$, $z$: Cartesian coordinates, m.

*Greek Symbols*

$\beta_t$: Coefficient, $(2-\sigma_t)\cdot 2\cdot k/[\sigma_t\cdot \mathrm{Pr}\cdot(K+1)]$
$\beta_v$: Coefficient, $(2-\sigma_v)/\sigma_v$
$\gamma$: Aspect ratio, $b/a$
$\theta$: Dimenpsionless fluid temperature
$\lambda$: Fluid thermal conductivity, W/(mK)
$\lambda_{\mathrm{mfp}}$: Mean free path of the fluid particles, m
$\mu$: Fluid dynamic viscosity, Pa s
$\xi$, $\psi$, $\zeta$: Dimensionless Cartesian coordinates
$\rho$: Fluid density, kg/m$^3$
$\sigma_T$: Thermal accomodation coefficient
$\sigma_v$: Momentum accomodation coefficient
$\tau$: Average wall shear stress, Pa.

*Subscripts*

*b*: Bulk
*j*: Jump at the wall
*s*: Slip at the wall
*w*: Wall.

## Acknowledgment

This work has been carried out thanks to the financial support of the PRIN2009TSYPM7_001 project "Single-phase and two-phase heat transfer for microtechnologies. Heat transfer and fluid flow in microscale."

## References

[1] E. B. Arkilic, K. S. Breuer, and M. A. Schmidt, "Gaseous flow in microchannels," in *Proceedings of the 1994 International Mechanical Engineering Congress and Exposition*, pp. 57–66, November 1994.

[2] E. B. Arkilic, M. A. Schmidt, and K. S. Breuer, "Gaseous slip flow in long microchannels," *Journal of Microelectromechanical Systems*, vol. 6, no. 2, pp. 167–178, 1997.

[3] T. Araki, M. S. Kim, I. Hiroshi, and K. Suzuki, "An experimental investigation of gaseous flow characteristics in microchannels," in *Proceedings of the International Conference on Heat Transfer and Transport Phenomena in Microscale*, pp. 155–161, Begell House, New York, NY ,USA, 2000.

[4] G. L. Morini, "Single-phase convective heat transfer in microchannels: a review of experimental results," *International Journal of Thermal Sciences*, vol. 43, no. 7, pp. 631–651, 2004.

[5] J. Liu, Y. C. Tai, and C. M. Ho, "MEMS for pressure distribution studies of gaseous flows in microchannels," in *Proceedings of the IEEE Micro Electro Mechanical Systems Conference*, pp. 209–215, Amsterdam, The Netherlands, February 1995.

[6] K. M. Sushanta and S. Chakraborty, *Microfluidics and Nanofluidics Handbook—Chemistry, Physics, and Life Science—Principles*, CRC Press, 2011.

[7] E. H. Kennard, *Kinetic Theory of Gases*, McGraw-Hill, New York, NY, USA, 1938.

[8] A. K. Sreekanth, "Slip flow through long circular tubes," in *Proceedings of the 6th International Symposium on Rarefied Gas Dynamics*, L. Trilling and H. Y. Wachman, Eds., pp. 667–680, Academic Press, New York, NY, USA, 1969.

[9] R. W. Barber and D. R. Emerson, "A numerical investigation of low Reynolds number gaseous slip flow at the entrance of circular and parallel plate micro-channels," in *Proceedings of the European Conference on Computational Fluid Dynamics (ECCOMAS '01)*, September 2001.

[10] W. A. Ebert and E. M. Sparrow, "Slip flow in rectangular and annular ducts," *ASME Journal of Basic Engineering*, vol. 87, pp. 1018–1024, 1965.

[11] Z. Duan and Y. S. Muzychka, "Slip flow in non-circular microchannels," *Microfluidics and Nanofluidics*, vol. 3, no. 4, pp. 473–484, 2007.

[12] G. L. Morini and M. Spiga, "Slip flow in rectangular microtubes," *Microscale Thermophysical Engineering*, vol. 2, no. 4, pp. 273–282, 1998.

[13] G. L. Morini, M. Spiga, and P. Tartarini, "The rarefaction effect on the friction factor of gas flow in microchannels," *Superlattices and Microstructures*, vol. 35, no. 3–6, pp. 587–599, 2004.

[14] G. L. Morini, M. Lorenzini, and M. Spiga, "A criterion for experimental validation of slip-flow models for incompressible rarefied gases through microchannels," *Microfluidics and Nanofluidics*, vol. 1, no. 2, pp. 190–196, 2005.

[15] S. Yu and T. A. Ameel, "Slip flow convection in isoflux rectangular microchannels," *Journal of Heat Transfer*, vol. 124, no. 2, pp. 346–355, 2002.

[16] C. Aubert and S. Colin, "High-order boundary conditions for gaseous flows in rectangular microducts," *Microscale Thermophysical Engineering*, vol. 5, no. 1, pp. 41–54, 2001.

[17] S. Colin, P. Lalonde, and R. Caen, "Validation of a second-order slip flow model in rectangular microchannels," *Heat Transfer Engineering*, vol. 25, no. 3, pp. 23–30, 2004.

[18] L. Ghodoossi and N. Eğrican, "Prediction of heat transfer characteristics in rectangular microchannels for slip flow regime and H1 boundary condition," *International Journal of Thermal Sciences*, vol. 44, no. 6, pp. 513–520, 2005.

[19] M. Renksizbulut, H. Niazmand, and G. Tercan, "Slip-flow and heat transfer in rectangular microchannels with constant wall temperature," *International Journal of Thermal Sciences*, vol. 45, no. 9, pp. 870–881, 2006.

[20] T. N. Aynur, L. Kuddusi, and N. Eğrican, "Viscous dissipation effect on heat transfer characteristics of rectangular microchannels under slip flow regime and H1 boundary conditions," *International Journal of Heat and Mass Transfer*, vol. 42, no. 12, pp. 1093–1101, 2006.

[21] L. Kuddusi and E. Çetegen, "Prediction of temperature distribution and Nusselt number in rectangular microchannels at wall slip condition for all versions of constant heat flux," *International Journal of Heat and Fluid Flow*, vol. 28, no. 4, pp. 777–786, 2007.

[22] L. Kuddusi and E. Çetegen, "Thermal and hydrodynamic analysis of gaseous flow in trapezoidal silicon microchannels," *International Journal of Thermal Sciences*, vol. 48, no. 2, pp. 353–362, 2009.

[23] L. Kuddusi, "First and second law analysis of fully developed gaseous slip flow in trapezoidal silicon microchannels considering viscous dissipation effect," *International Journal of Heat and Mass Transfer*, vol. 54, no. 1–3, pp. 52–64, 2011.

[24] Z. Duan and Y. S. Muzychka, "Slip flow in elliptic microchannels," *International Journal of Thermal Sciences*, vol. 46, no. 11, pp. 1104–1111, 2007.

[25] M. Bahrami, M. M. Yovanovich, and J. R. Culham, "Pressure drop of fully-developed, laminar flow in microchannel of arbitrary cross-section," *Journal of Fluids Engineering*, vol. 128, no. 5, pp. 1036–1044, 2006.

[26] M. Bahrami, M. Michael Yovanovich, and J. Richard Culham, "A novel solution for pressure drop in singly connected microchannels of arbitrary cross-section," *International Journal of Heat and Mass Transfer*, vol. 50, no. 13-14, pp. 2492–2502, 2007.

[27] Z. Duan and Y. S. Muzychka, "Models for gaseous slip flow in non-circular microchannels," in *Proceedings of the ASME/JSME Thermal Engineering Summer Heat Transfer Conference (HT '07)*, pp. 949–962, Vancouver, Canada, July 2007.

[28] Z. Duan and M. M. Yovanovich, "Pressure drop for laminar flow in microchannels of arbitrary cross-sections," in *Proceedings of the 25th Annual IEEE Semiconductor Thermal Measurement and Management Symposium (SEMI-THERM '09)*, pp. 111–120, San Jose, Calif, USA, March 2009.

[29] S. W. Churchill, *Viscous Flows, the Practical Use of Theory*, Butterworths, Boston, Mass, USA, 1987.